Journal of Applied Mechanics Vol.8, pp.73-84 (August 2005) JSCE

Structural damage identification algorithm based on changes in power spectral density

パワースペクトル密度の変化に基づく構造損傷同定アルゴリズム

Sherif Beskhyroun*, Toshiyuki Oshima**, Shuichi Mikami*** and Yutaka Tsubota ****
ベスキロウン シェリフ*, 大島俊之**, 三上修一***, 坪田豊****

*Doctoral Student, Dept. of Civil Eng., Kitami Institute of Technology, (165 Koen-cho, Kitami, 090-8507)
**Professor, Dept. of Civil Eng., Kitami Institute of Technology, (165 Koen-cho, Kitami, 090-8507)
***Associate Professor, Dept. of Civil Eng., Kitami Institute of Technology, (165 Koen-cho, Kitami, 090-8507)
****Research Associate, Dept. of Civil Eng., Kitami Institute of Technology, (165 Koen-cho, Kitami, 090-8507)

The occurrence of damage in a structure produces changes in its global dynamic characteristics such as its natural frequencies, mode shapes, modal dampings, modal participation factors, impulse response and frequency response functions. In this paper, a newly derived algorithm based on changes in power spectral density (PSD) is presented. The algorithm is used to detect damage, predict its location and assess the extent of damage in structures. The proposed method is based on only the measured data without the need for any modal identification. The method is described theoretically and applied to the experimental data, from a steel bridge model and bookshelf structure. Several damage scenarios were introduced to the members of the test structures. The method detected the damage, determined the exact location and monitored the increase in damage.

Key Words: damage detection, modal parameters, vibration data, health monitoring

1. Introduction

Most vibration-based damage detection theories and practices are formulated based on the assumption that failure or deterioration would primarily affect the stiffness and therefore affect the modal characteristics of the dynamic response of the structure. If this kind of changes can be detected and classified, this measure can be further implemented for a bridge monitoring system to indicate the condition, or damage, or remaining capacity of the structures. It can also be used to evaluate the seismic behavior of the structures. In recent years, there has been a renewed interest in the damage diagnosis and health monitoring of existing highway bridges. However, conventionally defined modal parameters have been shown to be mildly sensitive in the detection of various types of bridge damages. Furthermore, the modal parameters of conventional modal testing such as frequencies and modal dampings are global parameters, which cannot locate the damages. The experimental modal identification through ambient vibration measurements has become a very attractive technique nowadays. Ambient excitations such as traffic, wind, earthquakes, micro-vibration of the earth, and their combination are all natural or environmental agents. The ambient vibration has the advantage of being inexpensive and convenient since no equipment is needed to excite the structure. The service needs not have to be interrupted to use this technique. The experimental modal analysis by ambient vibrations was successfully applied to many bridges. One difficulty with determining dynamic parameters of a structure undergoing ambient vibrations is that the forcing function is not precisely characterized. Modal testing has some weaknesses as well. One of these is high level of noise, as compared with the signals.

Damage-detection methods such as acoustic or ultrasonic methods, magnetic field methods, radiograph, eddy-current methods and thermal field methods are either visual or localized experimental methods[1), 2)]. Unfortunately, they are all localized techniques, implying long and expensive inspection time; most often, structural components are not regularly inspected for no other reasons than their inaccessibility and damage can propagate to critical levels between inspection intervals. The drawbacks of current inspection techniques have led engineers to investigate new methods for continuous monitoring and global condition assessment of structures. That is the case for methods based on vibration responses that allow one to obtain meaningful time and/or frequency domain data and calculate changes in the structural and modal properties, such as resonance

frequencies, modal dampings and mode shapes. These properties are then used to develop reliable techniques to detect, locate and quantify damage[3]. Many damage detection schemes rely on analyzing response measurements from sensors placed on the structure[4-8]. Research efforts have been made to detect structural damage directly from dynamic response measurements in the time domain, e.g., the random decrement technique[9, 10], or from frequency response functions (FRF)[11]. Also, some damage detection methods have been proposed to detect damage using system identification techniques[12, 13].

In this paper, an algorithm based on changes in PSD is presented. The algorithm is used to detect damage, locate its position and monitor the increase in damage using only the measured data without the need for any modal identification. The method is applied to the experimental data extracted from a steel bridge model after inducing some defects to its members. The release of supporting bolts or the introduction of torch cut in the edge of some members introduced the damage to the bridge model. For further validation of the proposed method, it is also applied to the experimental data from a bookshelf structure. The damage in this case is introduced by releasing some bolts between the plates and columns of the bookshelf.

2. Theoretical description

2.1 Definition of Power Spectral Density

For a continuous time series, $x(t)$, defined on the interval of 0 to T, the Discrete Fourier Transform (DFT), $X(f)$, is defined as[14]

$$X(f)=\int_0^T x(t)e^{-i2\pi ft}dt \tag{1}$$

where $i=\sqrt{-1}$, and

f= cyclic frequency (Hz).

This function is complex and its magnitude is typically plotted in engineering units (EU), such as m/s^2 or g, versus frequency. The power spectrum is then defined as

$$|X(f)|^2 = X(f)X^*(f) \tag{2}$$

where * denotes a complex conjugate. The power spectrum is a real-valued frequency domain function with units of (EU)^2. The PSD, $G_x(f)$ is defined as

$$G_x(f)=\frac{2}{T}E\left[|X(f)|^2\right] \tag{3}$$

where $E[\ ]$ indicates an ensemble average for a specific f over n samples of $X(f)$. Again, this is a real-valued frequency domain function and has the units of (EU)$^2\cdot$ Hz. From the definition of PSD, it is noteworthy that PSD is calculated from the measured response of the structure such as the acceleration response without the need for measuring the excitation force. However, the excitation forces used for the undamaged and damaged structure must have the same amplitude and vibration wave form. Therefore, it is not necessary to measure the excitation force in order to use the ambient vibrations as an excitation source for continuous health monitoring of structures. On the other hand, the problem of obtaining two equal excitation forces from the ambient vibration data has not yet been solved.

2.2 Proposed algorithm

Let $G_i(f)$ denote the PSD magnitude measured at channel number i at frequency value f. The absolute difference in PSD magnitude before and after damage can then be defined as

$$D_i(f)=\left|G_i(f)-G_i^*(f)\right| \tag{4}$$

where $G_i(f)$ and $G_i^*(f)$ represent PSD magnitude for the undamaged and damaged structures respectively. When the change in PSD is measured at different frequencies on the measurement range from f_1 to f_m, a matrix $[D]$ can be formulated as follows

$$D=\begin{bmatrix} D_1(f_1) & D_1(f_2) & \cdots & D_1(f_m) \\ D_2(f_1) & D_2(f_2) & \cdots & D_2(f_m) \\ \cdot & \cdot & \cdots & \cdot \\ \cdot & \cdot & \cdots & \cdot \\ \cdot & \cdot & \cdots & \cdot \\ D_n(f_1) & D_n(f_2) & \cdots & D_n(f_m) \end{bmatrix} \tag{5}$$

where n represents the number of measuring points. In matrix $[D]$, every column represents the changes in PSD at different measuring channels but at the same frequency value. The summation of PSD changes over different frequencies can be used as the indicator of damage occurrence and the increase in damage. In other words, the first damage indicator is calculated from the sum of rows of matrix $[D]$ as

$$Total\_Change=\begin{Bmatrix} \sum_f D_1(f) \\ \sum_f D_2(f) \\ \cdot \\ \cdot \\ \cdot \\ \sum_f D_n(f) \end{Bmatrix}. \tag{6}$$

However it was found to be a weak indicator of damage localization. A statistical decision making procedure is employed to determine the location of damage. The first step in this procedure is the picking of the maximum change in PSD at each frequency value (the maximum value in each column of matrix $[D]$) and removing all other changes in PSD measured at other nodes. For example in matrix $[D]$, if $D_3(f_1)$ is the maximum value in the first column then this value will be used as $M_3(f_1)$ and other values in this column will be removed. The same process is applied to the different columns in matrix $[D]$ to formulate the matrix of maximum changes of PSD at different frequencies, $[M]$

$$M=\begin{bmatrix} 0 & 0 & 0 & \cdots & 0 \\ 0 & M_2(f_2) & 0 & \cdots & 0 \\ M_3(f_1) & 0 & 0 & \cdots & M_3(f_m) \\ 0 & 0 & M_4(f_3) & \cdots & 0 \\ \cdot & \cdot & \cdot & \cdots & \cdot \\ \cdot & \cdot & \cdot & \cdots & \cdot \\ 0 & 0 & 0 & \cdots & 0 \end{bmatrix}. \tag{7}$$

In order to monitor the frequency of damage detection at any node, a new matrix [C] is formulated. The matrix consists of 0's at the undamaged locations and 1's at the damaged locations. For example in the matrix [C], we put a value of 1 corresponding to the locations of $M_3(f_1)$, $M_2(f_2)$ and so on, as shown in the following expression

$$C=\begin{bmatrix} 0 & 0 & 0 & \ldots\ldots & 0 \\ 0 & 1 & 0 & \ldots\ldots & 0 \\ 1 & 0 & 0 & \ldots\ldots & 1 \\ 0 & 0 & 1 & \ldots\ldots & 0 \\ . & . & . & \ldots\ldots & . \\ . & . & . & \ldots\ldots & . \\ 0 & 0 & 0 & \ldots\ldots & 0 \end{bmatrix}. \tag{8}$$

The total of maximum changes in PSD can be calculated from the sum of the rows of matrix [M] as

$$SM=\begin{Bmatrix} \sum_f M_1(f) \\ \sum_f M_2(f) \\ . \\ . \\ . \\ \sum_f M_n(f) \end{Bmatrix}. \tag{9}$$

The total number of instances of detecting the damage at different nodes is calculated from the sum of the rows of matrix [C] as

$$SC=\begin{Bmatrix} \sum_f C_1(f) \\ \sum_f C_2(f) \\ . \\ . \\ . \\ \sum_f C_n(f) \end{Bmatrix}. \tag{10}$$

In order to reduce the effect of noise or measurement errors, a value of one or two times standard deviation of the elements in vector {SM} will be subtracted from the vector {SM}. Any resulting negative values will be removed. The same procedure will be applied to the vector {SC} as follows

$$SMD1=\begin{Bmatrix} \sum_f M_1(f)-\sigma \\ \sum_f M_2(f)-\sigma \\ . \\ . \\ . \\ \sum_f M_n(f)-\sigma \end{Bmatrix} \text{ or } SMD2=\begin{Bmatrix} \sum_f M_1(f)-2\sigma \\ \sum_f M_2(f)-2\sigma \\ . \\ . \\ . \\ \sum_f M_n(f)-2\sigma \end{Bmatrix} \tag{11}$$

where $\sigma=\sqrt{\sum_{i=1}^{n}(SM(i)-\overline{SM})^2}\Big/(n-1)$, $\overline{SM}=\sum_{i=1}^{n}SM(i)\Big/n$,

$$SCD1=\begin{Bmatrix} \sum_f C_1(f)-\lambda \\ \sum_f C_2(f)-\lambda \\ . \\ . \\ . \\ \sum_f C_n(f)-\lambda \end{Bmatrix} \text{ or } SCD2=\begin{Bmatrix} \sum_f C_1(f)-2\lambda \\ \sum_f C_2(f)-2\lambda \\ . \\ . \\ . \\ \sum_f C_n(f)-2\lambda \end{Bmatrix} \tag{12}$$

where $\lambda=\sqrt{\sum_{i=1}^{n}(SC(i)-\overline{SC})^2}\Big/(n-1)$, $\overline{SC}=\sum_{i=1}^{n}SC(i)\Big/n$.

The damage indicator is defined as the scalar product of {SMD} and {SCD} as shown in the following expressions

$$Damage\_Indicator\_1=\begin{Bmatrix} SMD1(1)\times SCD1(1) \\ SMD1(2)\times SCD1(2) \\ . \\ . \\ . \\ SMD1(n)\times SCD1(n) \end{Bmatrix}, \tag{13}$$

$$Damage\_Indicator\_2=\begin{Bmatrix} SMD2(1)\times SCD2(1) \\ SMD2(2)\times SCD2(2) \\ . \\ . \\ . \\ SMD2(n)\times SCD2(n) \end{Bmatrix}. \tag{14}$$

Damage indicators 1 and 2 will be used to determine the damage location. On the other hand, the total change in PSD (Eq. (6)) will be used to detect the occurrence of damage and assess the damage extent.

3. Steel bridge model

3.1 Experimental setup and equipment

In this research, a steel bridge model is examined after inducing damage with different levels to some members. The model consists of two girders and six cross beams. Each cross beam is connected to the girders with four bolts, 2 bolts in each side. The model dimensions and layout are shown in Figs. 1 and 2. The multi-layer piezoelectric actuator is used for local excitation. The main advantage of using piezoelectric actuator is that it produces vibration with different frequencies ranging from 0.1 to 400 Hz that is effective in exciting different mode shapes[15),16)]. Five natural frequencies are measured in the range of the excitation frequency (from 0.1 to 400 Hz) at 43.75, 118.85, 212.5, 300, 393.75 Hz. The actuator force amplitude is 0.2 kN. The actuator is located at the center of the upper flange of the main girder (Figs. 1 and 2). The location of the actuator is not changed during different damage states of the structure. The effects of changing the actuator location on the accuracy of the results are not studied in this research. The excitation forces used for the undamaged and damaged structure are random, equal in amplitude and have the

same vibration wave form but the excitation force does not need to be measured. One accelerometer is mounted at the bottom of each cross beam to measure the acceleration response in the vertical direction at the mid span of each cross beam, as shown in Fig. 2.

Seven cases of damage are introduced to the specimen as follows:

Case 1: Removing one bolt completely from the left side of cross beam no. 2 (Fig. 3).

Case 2: Case 1 + releasing one bolt at the left side of cross beam no. 2 (Fig. 3).

Case 3: Case 2 + removing one bolt at the right side of cross beam no. 2 (Fig. 3).

Case 4: Case 3 + releasing one bolt at the right side of cross beam no. 2 (Fig. 3).

Case 5: Removing one bolt from the left side of cross beam no. 3.

Case 6: Removing one bolt and releasing the second one from the left side of cross beam no. 2. The same damage is introduced to cross beam no. 5.

Case 7: A torch cut of 20 mm length and 1 mm width is introduced at the middle of cross beam no. 2. The cut starts from the edge of the horizontal plate of the beam.

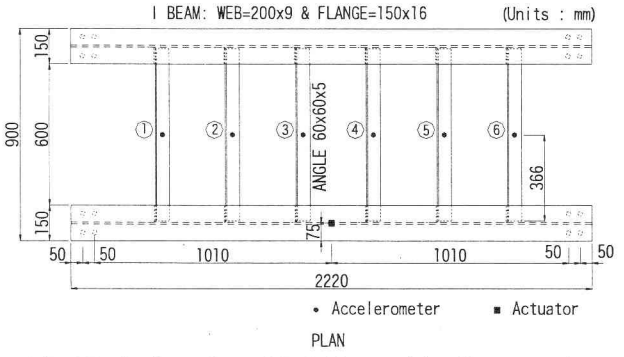

Fig. 1 Basic dimensions of the bridge model and beam numbers

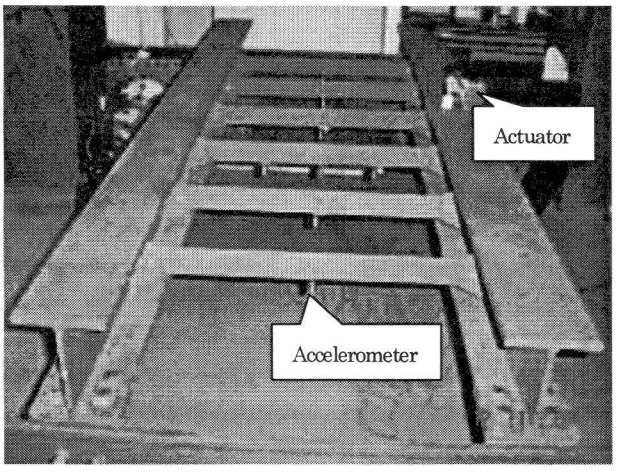

Fig. 2 Accelerometers and actuator positions

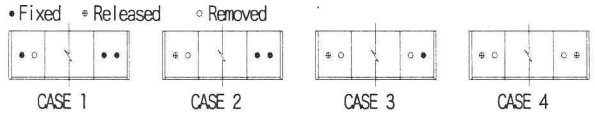

Fig. 3 Damage cases introduced to cross beam no. 2

3.2 Damage identification algorithm applied to different damage cases for the steel bridge model

(1) Estimation of PSD data

The PSD is calculated from node point accelerations using MATLAB[17), 18)] standard and the MATLAB Signal Processing Toolbox as follows: $G_i(f)$ = PSD ($x(t)$, NFFT, Fs, WINDOW) estimates the power spectral density of a discrete-time signal vector $x(t)$ using Welch's averaged, modified periodogram method[19),20),21)]. $x(t)$ is divided into overlapping sections, each of which is detrended (according to the detrending flag, if specified), then windowed by the WINDOW parameter, then zero-padded to length NFFT where NFFT specifies the DFT length that PSD uses. The magnitude squared of the length NFFT DFTs of the sections are averaged to form $G_i(f)$. Then 10 is multiplied to the base 10 logarithm of the elements of $G_i(f)$ to compute $G_i(f)$ in (dB). $G_i(f)$ is length NFFT/2+1 for NFFT even, (NFFT+1)/2 for NFFT odd.. If a scalar for WINDOW is specified, a Hanning window of that length is used. Fs is the sampling frequency which does not affect the spectrum estimate but is used for scaling the X-axis of the plots. In this study, WINDOW = NFFT = 256 and Fs = 1600.

(2) Before introducing any damage

One of the drawbacks of vibration based damage identification methods is that these methods sometimes produce false positive readings due to noise, measurement errors or environmental changes. It is therefore very important to determine if the results obtained from any damage identification method are due to damage or due to other changes. Because of this need, the experiment was performed a number of times on the undamaged structure prior to the introduction of any damage. PSD data for two different sets of data obtained from the undamaged structure is shown in Fig. 4. Small changes in PSD can be observed in this figure, obviously due to noise and measurement errors. PSD data in the frequency range of 50–700 Hz was used for the proposed method. The total change in PSD was determined using Eq. (6) and the results are shown in Fig. 5. The total change in PSD ranged from about 60 to 90 dB. When the total change of PSD was determined using other sets of data that were obtained from the undamaged structure, similar and very close values of the total change in PSD were obtained. The total change of PSD will be used as an indicator of damage detection and damage increase. On the other hand, damage indicators 1 and 2 will be used to identify the damage location.

(3) Cases 1, 2, 3 and 4 (damage at beam no. 2)

The accuracy of the damage identification methods based on FRF or cross spectral density (CSD) is dependent on the frequency range in which FRF[3)] or CSD[22)] is measured. The accuracy of the damage identification methods based on mode shapes is dependent on which mode shapes are used. The accuracy of the results is sometimes reduced when some of the used mode shapes have nodes at the damage location[2)]. In order to overcome this problem, it was decided

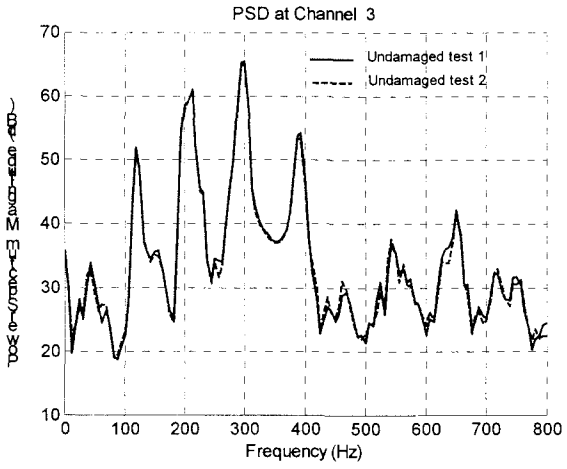

Fig. 4 PSD for two tests performed on the undamaged structure

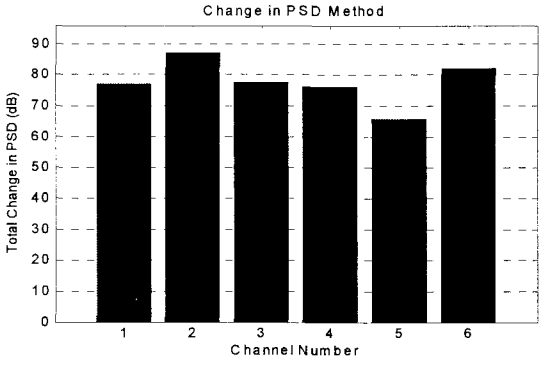

Fig. 5 Total change in PSD due to noise

to use PSD magnitudes in the frequency range of 50–700 Hz in the proposed algorithm. This range of measurement covers most of the total measurement range of PSD data (from 0 to 800 Hz). Only a small range of measurements at the beginning (from 0 to 50 Hz) and at the end (from 700 to 800 Hz) was not used in order to avoid the low-frequency noise and the higher frequency modes. The resulting damage indicators for the four levels of actual damage – damage cases 1 through 4, are plotted in Figs. 6 to 9. In Fig. 6 (a), the total change in PSD (Eq. (6)) increased at all channels after removing the first bolt. The total change in PSD due to the removal of one bolt is much larger than that due to noise and measurement errors (Fig. 5). Although the maximum total change of PSD is observed at channel 2 (the damage location), the total change in PSD is not always a good indicator of damage location as will be noticed in the bookshelf structure. Damage indicators 1 and 2 have determined the damage location at channel 2 accurately, as shown in Figs. 6 (b) and 6 (c), respectively. After increasing the damage level in beam no. 2, the same previous remarks were also observed. As clearly indicated in Figs. 7 to 9, the damage at beam no. 2 was located accurately using both damage indicators 1 and 2 without any false positive readings. The total changes in PSD (Eq. (6)) for the four cases of damage and for the intact structure are plotted in Fig. 10. The following remarks can be drawn from this figure:

- The total change in PSD due to noise is less than 100 dB at all channels with close values at the different channels.
- After removing the first bolt (Case 1), the total change in PSD increased slightly at the undamaged locations (damage at one location will change the overall stiffness of the structure) and increased remarkably at the damaged location (channel 2).
- After releasing one more bolt (Case 2), the total change in PSD continued to increase slightly at the undamaged locations and remarkably at the damaged location.
- After introducing damage to the third and fourth bolts (Cases 3 and 4), the total change in PSD increased slightly at the damaged location since the beam has already lost most of its stiffness after removing the second bolt.

Therefore, it can be concluded that the total change in PSD monitored the increase in damage successfully.

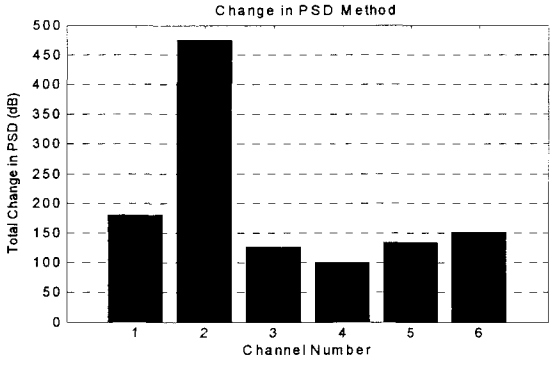

Fig. 6 (a) Total change in PSD

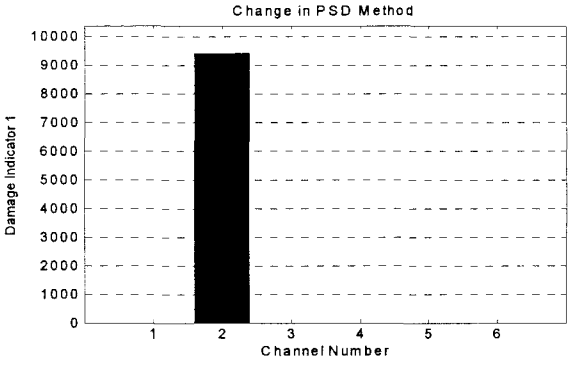

Fig. 6 (b) Damage localization results using damage indicator 1

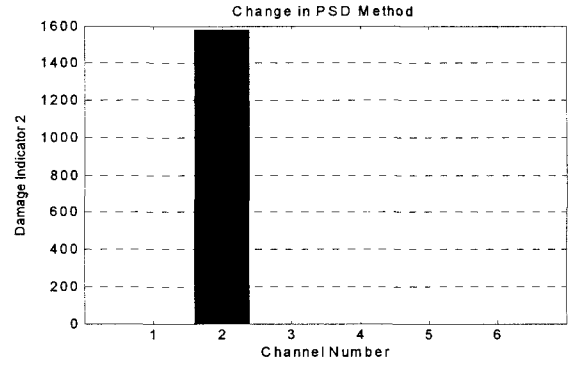

Fig. 6 (c) Damage localization results using damage indicator 2

Fig. 6 Proposed algorithm results for damage case 1

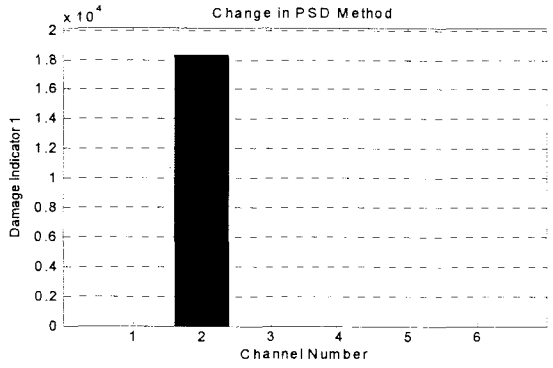

Fig. 7 (b) Damage localization results using damage indicator 1

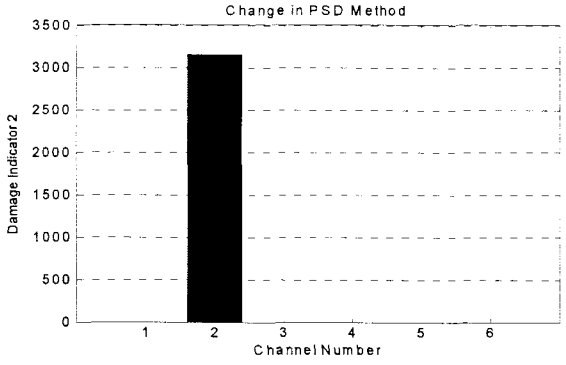

Fig. 7 (c) Damage localization results using damage indicator 2

Fig. 7 Proposed algorithm results for damage case 2

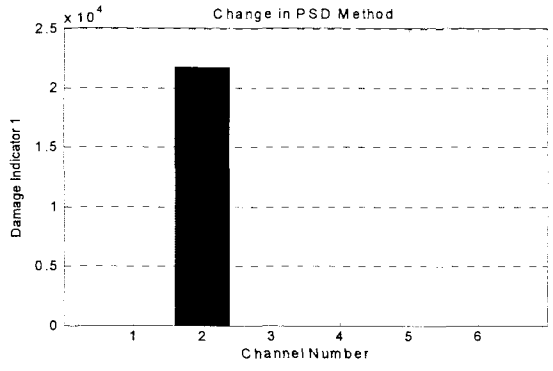

Fig. 8 (b) Damage localization results using damage indicator 1

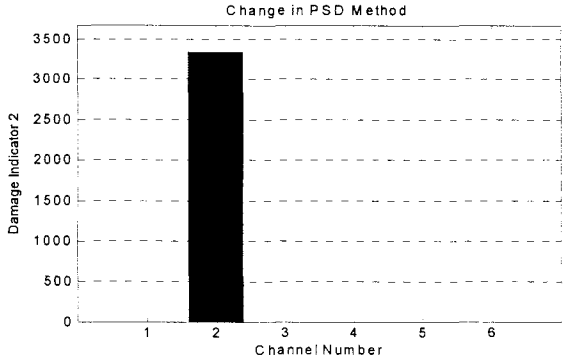

Fig. 8 (c) Damage localization results using damage indicator 2

Fig. 8 Proposed algorithm results for damage case 3

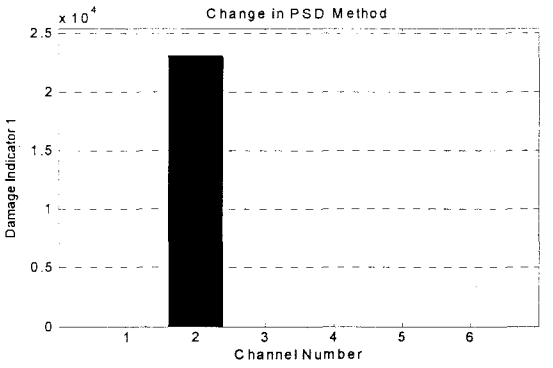

Fig. 9 (a) Damage localization results using damage indicator 1

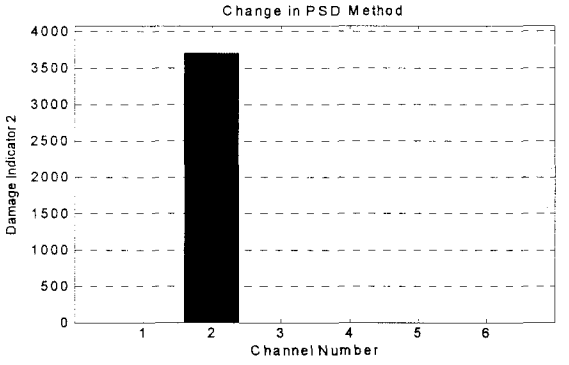

Fig. 9 (b) Damage localization results using damage indicator 2

Fig. 9 Proposed algorithm results for damage case 4

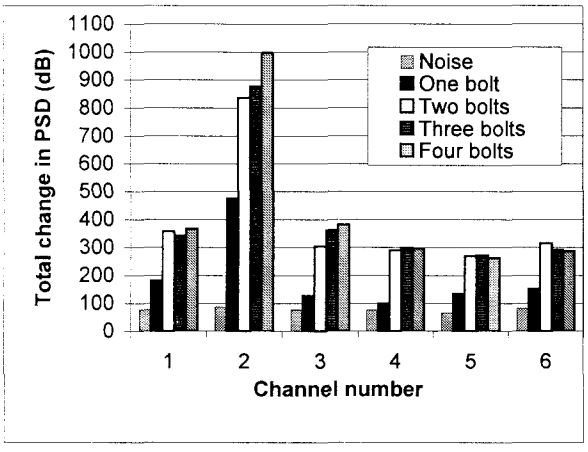

Fig. 10 Total change in PSD for different damage cases at beam no. 2

(4) Case 5 (damage at beam no. 3)

The accuracy of damage identification methods based on mode shapes is sometimes reduced when the damage exists at the node of the used modes. Therefore, the damage position is changed in this case to examine the effects of changing the damage position. The PSD magnitude is measured in the frequency range of 50–700 Hz. The results of this case are shown in Fig. 11. The damage is indicated accurately at channel 3 using both damage indicators 1 and 2. Damage indicator 1 has detected the damage at channel 3 with some very small values appearing at other channels (undamaged locations), as shown in Fig. 11(a). On the other hand, damage indicator 2 has

detected the damage accurately without any readings at the undamaged locations Fig. 11(b). Damage indicator 2 performed better for this case than damage indicator 1.

(5) Case 6 (damage at beams no. 2 and 5)

This case is introduced to investigate the feasibility of the algorithm to detect multiple-damage. The PSD magnitude is measured in the frequency range of 50–700 Hz. Damage at the two positions is detected and localized accurately with no false positive readings using damage indicator 1, as shown in Fig. 12(a). As indicated in this figure, the damage indicator value at channel 2 is higher than that at channel 5. This difference is due to the fact that the structure is not exactly symmetrical, the fixation of the bolts in the two angles (2 and 5) is not exactly the same and moreover the amount of noise or measurement errors stored in the data of each measuring channel is not equal. Damage indicator 2 detected the damage at channel no. 2 only because the filtering of the data is bigger than that for damage indicator 1. The obtained results from case 5 and case 6 indicate that damage indicator 2 gives better results for the cases of single damage with lower chance for false positive readings to appear. On the other hand, damage indicator 1 performed better in case of multiple-damage. This result will be illustrated in more details when the method is applied to the bookshelf structure.

(6) Case 7 (crack at beams no. 2)

Case 7 is introduced to investigate the feasibility of the algorithm to detect different types of damages. The PSD magnitude is measured in the same frequency range of 50–700 Hz. Damage at channel 2 is detected and localized accurately with no false positive readings, as shown in Fig. 13. It was noticed that the total change in PSD for this case was smaller than the case of removing one bolt (Case 1), which means that detecting the damage in this case was more difficult than the case of bolt release. This is because the effect of removing any bolt on the vibration response of the beam is greater than the case of localized crack. When the method was applied to detect a crack length of 10 mm at same location of this case, inaccurate results in identifying the damage were obtained.

4. Bookshelf structure

The experimental work on the bookshelf structure was done by Charles R. Farrar and David V. Jauregui of Los Alamos National Laboratory (LANL), U.S.A. The data is available through the internet on the LANL site[23]. The tested structure is a three-story frame structure model as shown in Fig 14. It is constructed of aluminum box columns and aluminum floor plates. The floors are 1.3 cm thick aluminum plates with two-bolt connections to brackets on the column. The base is a 3.8 cm thick aluminum plate. Support brackets for the columns are bolted to this plate and hold the columns. Dimensions of the test structure are displayed in Figs. 15 and 16. All bolted connections are tightened to a torque of 6.77 N.m in the undamaged state. Four air mount isolators, which allow the structure to move

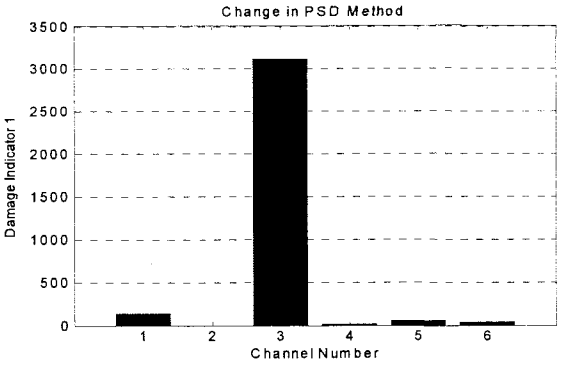

Fig. 11 (a) Damage localization results using damage indicator 1

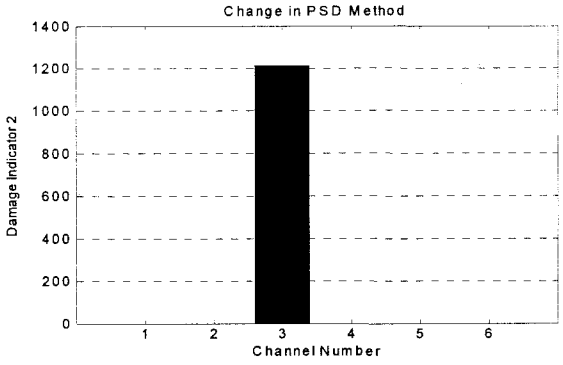

Fig. 11 (b) Damage localization results using damage indicator 2

Fig. 11 Proposed algorithm results for damage case 5

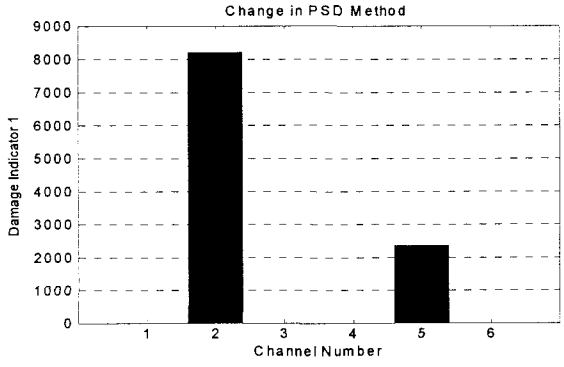

Fig. 12 (a) Damage localization results using damage indicator 1

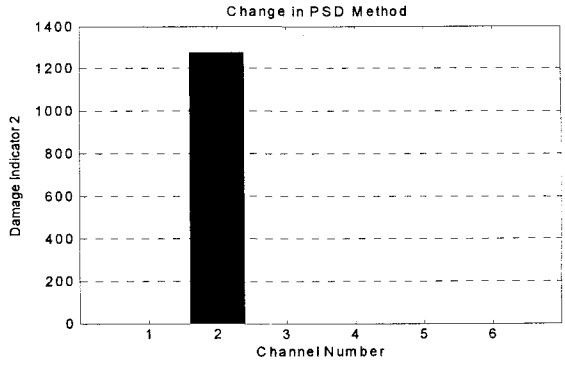

Fig. 12 (b) Damage localization results using damage indicator 1

Fig. 12 Proposed algorithm results for damage case 6

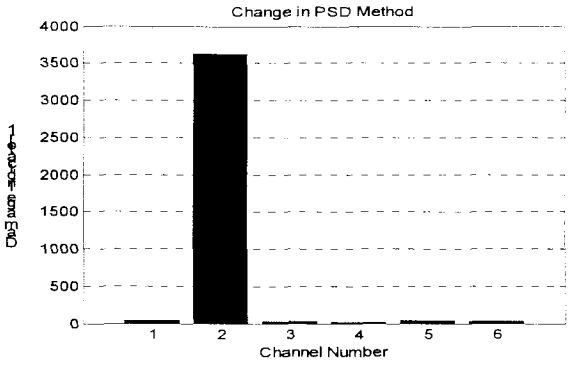

Fig. 13 (a) Damage localization results using damage indicator 1

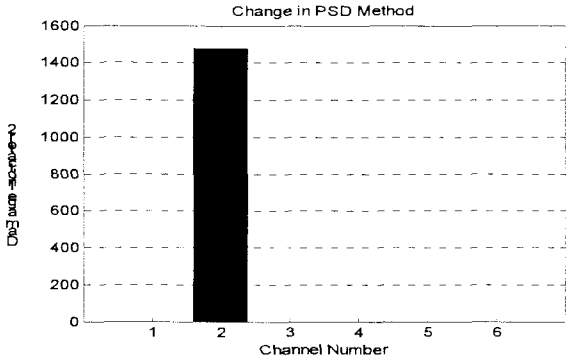

Fig. 13 (b) Damage localization results using damage indicator 2

Fig. 13 Proposed algorithm results for damage case 7

freely in horizontal directions, are bolted to the bottom of the base plate. Air mount isolators use a contained column of air inside an elastomeric bellows or sleeve to buffer cyclic motion, provide vibration isolation. They incorporate a carefully designed rubber and fabric bellows that contains a column of compressed air. The rubber bellows itself does not provide force or support load - the column of air does this when the air spring is inflated according to the load required of it. The isolators are inflated to 140 kPa gauge and then adjusted to allow the structure to sit at the same level with the shaker. The shaker is coupled to the structure by a 15 cm long, 9.5-mm diameter stinger connected to a tapped hole at the mid-height of the base plate. The shaker is attached at corner D as shown in Fig. 16, so that both translational and torsional motions can be excited.

4.1 Test setup and data acquisition

The structure is instrumented with 24 piezoelectric single axis accelerometers, two per joint as shown in Fig. 16. Accelerometers are mounted on the aluminum blocks that are attached by hot glue to the plate and column. This configuration allows relative motion between the column and the floor to be detected. The nominal sensitivity of each accelerometer is 1 V/g. A commercial data acquisition system controlled from a laptop PC is used to digitize the accelerometer analog signals. The data sets that were analyzed in the feature extraction and statistical modeling portion of the study were the acceleration time histories. In the damaged cases, the bolts at the joint indicated were loosened and then tightened again to hand tight allowing the plate to move relative to the column. All input from the shaker to the base was random. In each test case, the data sets were collected with the shaker input level kept at 8 volts. The bandwidth of the shaker and response were also kept at equal values for different test cases. Each time signal gathered consisted of 8192 points and were sampled at 1600 Hz. Channels 1-24 represent the accelerometers placed on the structure. Channels 1 and 2 represent the first pair of sensors across a joint, 3 and 4 are the next and so on. Each sensor position is marked with either a P (Plate) or C (column) to indicate the position relative to the joint. Channel number and the corresponding position are shown in Table (1). The following damage cases are introduced to the bookshelf structure:

Case 1: Damage location is 1C (floor 1, corner C). The bolts between the bracket and the plate are left in at a torque value of 1.128 N.m.

Case 2: Damage location is 1C (floor 1, corner C). The bolts between the bracket and the plate are left in at a torque value of 0.564 N.m.

Case 3: Damage location is 1C (floor 1, corner C). The bolts are left in at a hand tight torque.

Case 4: Damage location is 3A (floor 3, corner A). The bracket is completely removed.

Case 5: Damage locations are 3A and 1C. The bolts are removed between the bracket and the plate at both damage locations.

4.2 Damage identification algorithm applied to different damage cases for the bookshelf structure

(1) Cases 1, 2 and 3 (channels 21 and 22)

In damage cases 1, 2 and 3, damage is located at 1C. Therefore channels 21 and 22 are the nearest sensors to the damage location as shown in Table (1). PSD magnitude in the frequency range of 50–700 Hz was used in the proposed algorithm.

Case 1 represents the smallest damage introduced to the bookshelf structure. Fig. 17 (a) shows the total change in PSD as determined from Eq. (6). As clearly indicated in this figure, the damage location cannot be determined using this indicator as explained in section 2.2. Damage indicator 1 located the damage accurately at channel 22 however some small values appeared at undamaged locations as shown in Fig. 17 (b). Damage indicator 2 detected the damage without any readings at the undamaged locations (Fig. 17 (c)). The same remark was observed in case 5 for the bridge model.

In case 2, the torque left in bolts between the bracket and the plate at location 1C was reduced to the half of its value of case 1. Damage indicators 1 and 2 detected the damage locations at channels 21 and 22 more accurately than in case 1 as indicated in Fig. 18. Although damage increased in this case compared to case 1, damage indicators values decreased compared to their values in case 1. Therefore damage indicators 1 and 2 are used to locate the damage position but cannot be used to monitor the increase in damage. This is because only the maximum change in PSD magnitude at each frequency is used and other values are removed. On the other hand, the total change in PSD can be used to monitor the increase in damage.

In case 3, damage increased slightly at location 1C as compared to

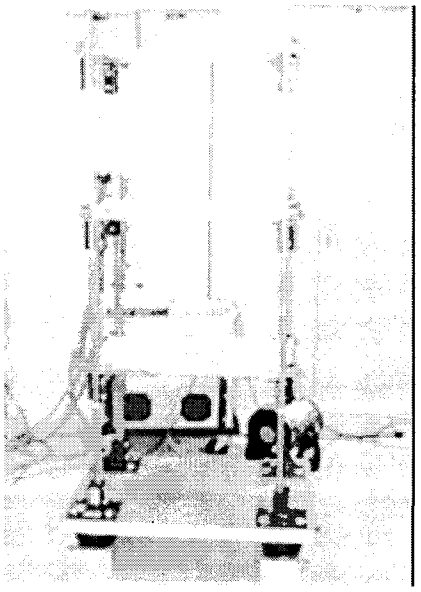

Fig. 14 Photo of the full test structure

Table 1 Channel position

Ch.	Posit.
1	3BP
2	3BC
3	3AP
4	3AC
5	3CP
6	3CC
7	3DP
8	3DC
9	2BP
10	2BC
11	2AP
12	2AC
13	2CP
14	2CC
15	2DP
16	2DC
17	1BP
18	1BC
19	1AP
20	1AC
21	1CP
22	1CC
23	1DP
24	1DC

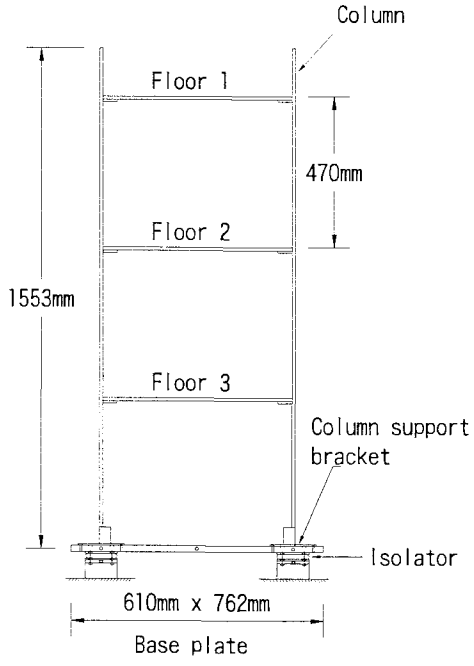

Fig. 15 Basic dimensions of the 3 story frame structure

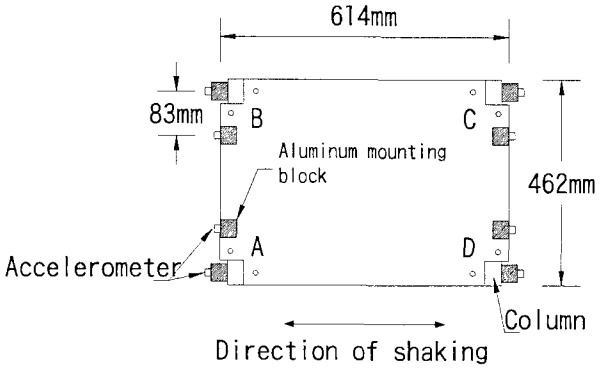

Fig. 16 Floor layout as viewed from above

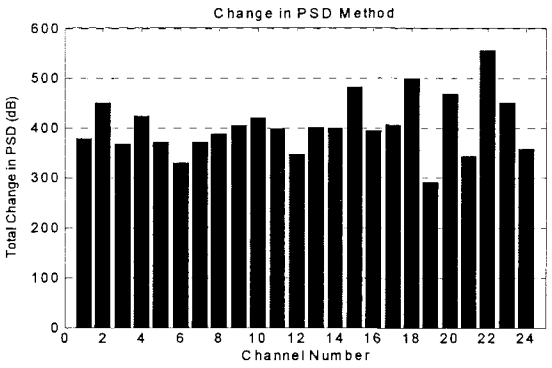

Fig. 17 (a) Total change in PSD

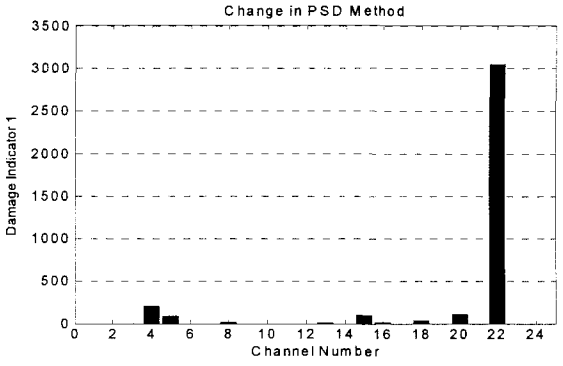

Fig. 17 (b) Damage localization results using damage indicator 1

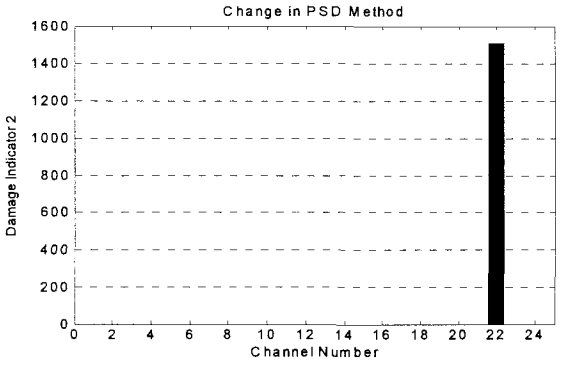

Fig. 17 (c) Damage localization results using damage indicator 2

Fig. 17 Proposed algorithm results for damage case 1 at location 1C

case 2. Both damage indicators 1 and 2 detected the damage locations at channels 21 and 22 accurately, as shown in Fig. 19.

Fig. 20 shows the total change in PSD for cases 1, 2 and 3. The total change in PSD obtained from two different tests performed on the undamaged structure are also shown in the same figure and indicated by the legend noise. As clearly indicated in this figure, the total change in PSD increases as the damage level increases. The total change in PSD increased at all channels due to the presence of damage at location 1C. The same observations were also noticed for the bridge model structure.

(2) Case 4 (channels 3 and 4)

In case 4, damage is located near channels 3 and 4. PSD magnitude is measured in the frequency range of 50–700 Hz as for

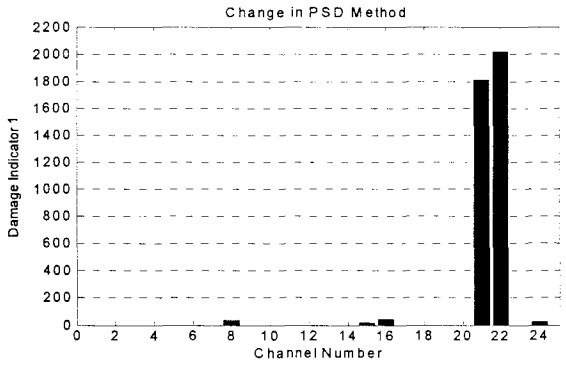

Fig. 18 (a) Damage localization results using damage indicator 1

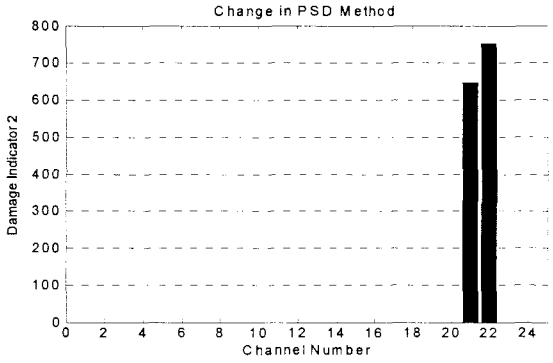

Fig. 18 (b) Damage localization results using damage indicator 2

Fig. 18 Proposed algorithm results for damage case 2 at location 1C

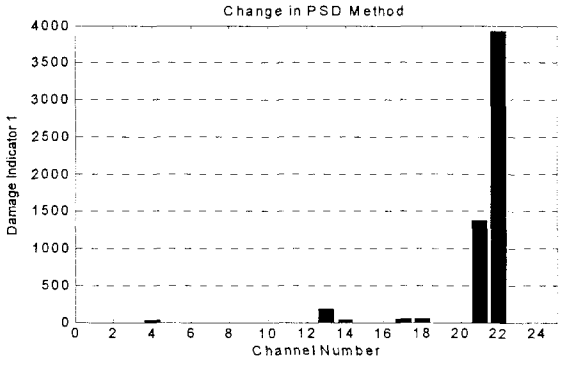

Fig. 19 (a) Damage localization results using damage indicator 1

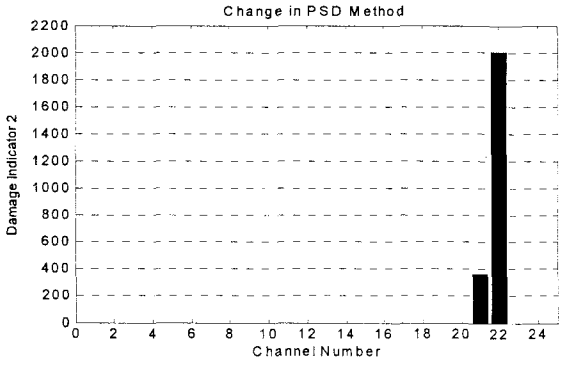

Fig. 19 (b) Damage localization results using damage indicator 2

Fig. 19 Proposed algorithm results for damage case 3 at location 1C

the previous cases. Damage is located accurately at channel 4 using both damage indicators 1 and 2, as shown in Fig. 21. When the damage level increased at location 3A from level 1 (the bolts were removed between the bracket and the plate) to level 2 (the bracket was completely removed), the increase in damage could be monitored successfully using the total change in PSD, as indicated in Fig. 22.

(3) Case 5 (channels 3, 4, 21 and 22)

Case 5 is introduced to investigate the feasibility of the algorithm

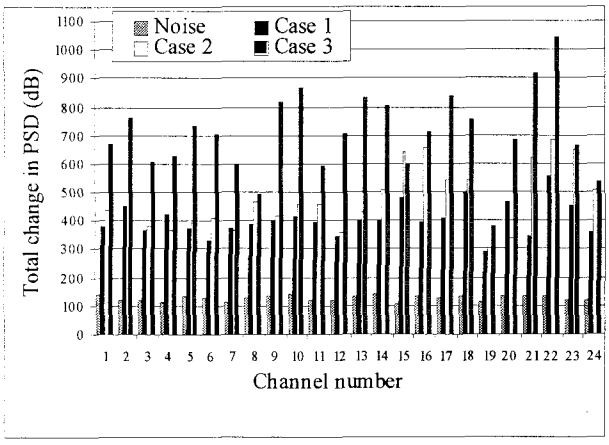

Fig. 20 Total change in PSD for different damage cases at location 1C (channels 21 and 22)

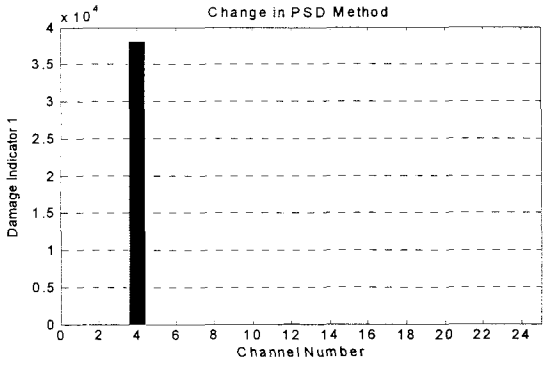

Fig. 21 (a) Damage localization results using damage indicator 1

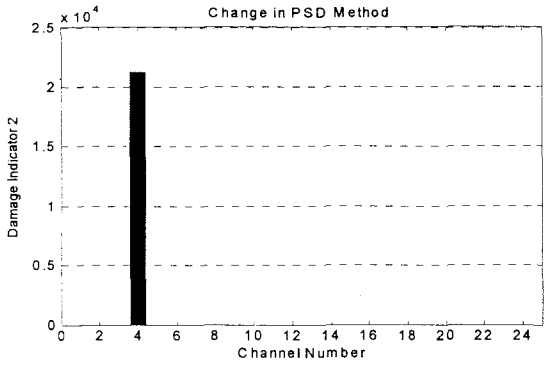

Fig. 21 (b) Damage localization results using damage indicator 2

Fig. 21 Proposed algorithm results for damage case 4 at location 3A

to detect multiple-damage. The PSD magnitude is measured in the frequency range of 50–500 Hz. Damage is located near the channels no. 3, 4, 21 and 22. Damage at the two positions is detected and localized accurately, using both damage indicators, as shown in Fig. 23. When the PSD was measured in the frequency range of 50–700 Hz, the damage indicator value at channel 22 was much higher than its value at channel 3 in a way that reduced the appearance of the bar at channel 3, especially in case of using damage indicator 2.

Comparing the results of damage indicators 1 and 2 obtained from the bridge model and bookshelf structure, the following remarks can be made: damage indicator 2 usually gives better results for the cases of single damage with fewer false positive readings than damage indicator 1. This is because the filtering of the data is more severe in case of damage indicator 2 (compare $SMD1$ to $SMD2$ in Eq. (11) and $SCD1$ to $SCD2$ in Eq. (12)). On the other hand in cases of multiple-damage, damage indicator 2 sometimes determines the damage at one location and does not determine the damage at other locations. This is because the acute filtering of the data in case of using damage indicator 2 sometimes removes the indication of damage at some locations. Therefore, it is necessary to apply both damage indicators to the data in order to confirm the correct locations of damage.

5. Conclusions

Changes in the PSD magnitude due to the presence of structural damage have been investigated. The experimental results obtained from a steel bridge model and bookshelf structure demonstrate the usefulness of the changes in PSD magnitude as a diagnostic parameter in detecting the damage, locating its position and monitoring the increase in damage. The main advantages of the proposed methods are:

(1) PSD is calculated from the acceleration response at every channel without measuring the excitation force. Therefore, ambient vibration can be used as an excitation force for continuous health monitoring of structures. However, using different excitation forces for the undamaged and damaged structure needs further investigation.

(2) The proposed method encompasses the first three steps of the process of damage detection – existence, localization and monitoring the damage increase being based on only the measured data without the need for any modal identification.

(3) The accuracy of damage identification methods based on changes in mode shapes are sometimes reduced when the damage occurs at a node of the used mode shapes. And, the accuracy of damage identification methods based on changes in FRF or CSD are dependent on the measurement range in which FRF or CSD are measured. The proposed method overcomes this drawback by using PSD data in the total measured frequency range.

(4) Vibration based damage identification methods sometimes produce false positive readings due to measurement errors, noise and environmental changes. The proposed method has shown better results in identifying the changes in PSD associated with damage from the changes attributed to noise or measurement errors.

Acknowledgement

This research is supported by the Grant-in-Aids for Scientific Research, Ministry of Education. The authors wish to express their gratitude for this support. The authors would like to acknowledge Dr. Farrar and LANL for the authorization in using the photos, drawings and data of the bookshelf structure.

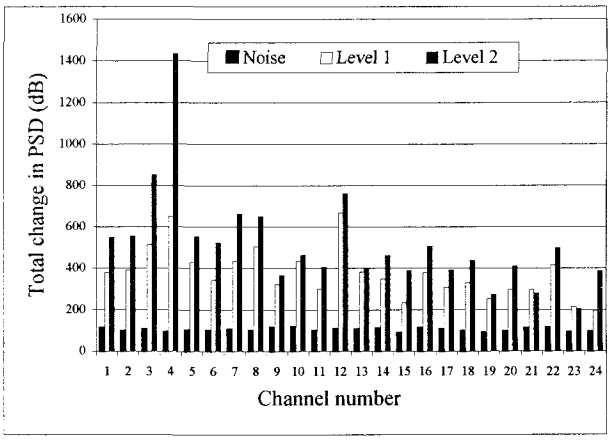

Fig. 22 Total change in PSD for different damage cases at location 3A (channels 3 and 4)

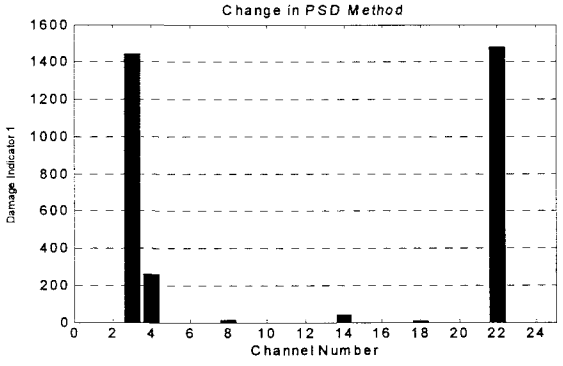

Fig. 23 (a) Damage localization results using damage indicator 1

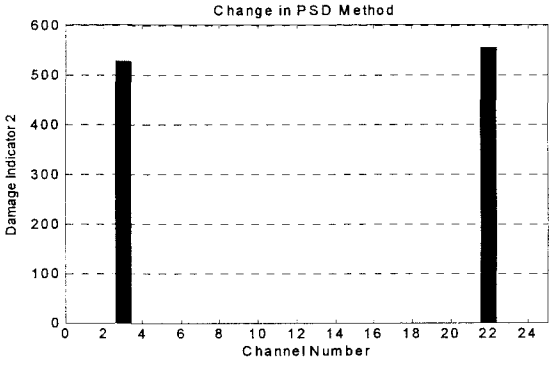

Fig. 23 (b) Damage localization results using damage indicator 2

Fig. 23 Proposed algorithm results for damage case 5 at locations 3A and 1C

References

1) Doebling S. W., C. R. Farrar, M. B. Prime, and D. W. Shevitz, *Damage Identification and Health Monitoring of Structural and Mechanical Systems from Changes in their Vibration Characteristics*, A Literature Review, Los Alamos National Laboratory Report, LA-13070- MS, 1996.
2) Farrar C. R. and D. A. Jauregui, *Damage Detection Algorithms Applied to Experimental and Numerical Model Data from the I-40 Bridge*, Los Alamos National Laboratory Report, LA-12979-MS, 1996.
3) Sampaio R. P. C., Maia N. M. M. and Silva J. M. M., Damage detection using the frequency-response-function curvature method, *Journal of Sound and Vibration*, 226(5), pp. 1029-1042, 1999.
4) Ojalvo, I.U., and Pilon, D., Diagnostics for Geometrically Locating Structural Math Model Errors from Modal Test Data, *Proc. of 29th AIAA/ASME/ASCE/ASC Structures, Structural Dynamics, and Materials Conference*, Williamsburg, VA, 1988.
5) Ricles, J.M., and Kosmatka, J.B., Damage Detection in Elastic Structures Using Vibratory Residual Forces and Weighted Sensitivity, *AIAA Journal*, Vol. 30, No. 9, pp. 2310-2316, 1992.
6) Smith, S.W., and Li, C., A Hybrid Approach for Damage Detection in Flexible Structures, *Proceedings of the 35th AIAA/ASME/ASCE/AHS/ASC Structures, Structural Dynamics, and Materials Conference*, pp. 285-293, AIAA-94-1710-CP, 1994.
7) Carrasco, C.J. Osegueda, R.A. and Ferregut, C.M, *Modal Tests of a Space Truss Model and Damage Localization Using Modal Strain Energy*, Report FAST 96-10 - FAST Center for Structural Integrity of Aerospace Systems, University of Texas El Paso, El Paso, Texas 79968-0516, July 1996.
8) Peeters B., Maeck J. and De Roeck G., Vibration-based damage detection in civil engineering: excitation sources and temperature effects, *Smart Materials and Structures*, 10, pp.518-527, 2001.
9) E. Kummer, J. C. S. Yang and N. G. Dagalakis, Detection of fatigue cracks in structural members, *2nd American Society of Civil Engineering/EMD Specialty Conference*, Atlanta, Georgia, 445-460, 1981.
10) J. C. S. Yang, J. Chen and N. G. Dagalakis, Damage detection in offshore structures by the random decrement technique, *Journal of Energy Resources Technology*, American Society of Mechanical Engineers 106, 38-42, 1984.
11) R. G. Flesch and K. Kernichler, Bridge inspection by dynamic tests and calculations dynamic investigations of Lavent bridge, *workshop on Structural Safety Evaluation Based on System Identification Approaches* (H. G. Natke and J. T. P. Yao, editors), 433-459, Lambrecht/ Pfalz, Germany: Vieweg & Sons, 1988.
12) S. F. Masri, R. K. Miller, A. F. Saud and T. K. Caughey, Identification of nonlinear vibrating structures, *Journal of Applied Mechanics 54*, 923-929: Part I-formulation, 1987.
13) H. G. Natke and J. T. P. Yao, System identification methods for fault detection and diagnosis, *International Conference on Structural Safety and Reliability*, American Society of Civil Engineers, New York, 1387-1393, 1990,
14) Farrar C. R. et al., *Dynamic Characterization and Damage Detection in the I-40 Bridge Over the Rio Grande*, A Literature Review, Los Alamos National Laboratory Report, LA-12767-MS, 1994.
15) Oshima T. et al., Study on damage evaluation of joint in steel member by using local vibration excitation, (In Japanese), *Journal of Applied Mechanics JSCE*, Vol.5, pp.837-846, 2002.
16) Beskhyroun S., Oshima T., Mikami S., Yamazaki T., Damage detection and localization on structural connections using vibration based damage identification methods, *Journal of Applied Mechanics, JSCE*, Vol.6, pp. 1055-1064, 2003.
17) MATLAB *Reference Guide*, The Math Works, Inc., Natick, MA, 2003.
18) MATLAB *User's Guide*, The Math Works, Inc., Natick, MA, 2003.
19) Hayes M., *Statistical Digital Signal Processing and Modeling*, John Wiley & Sons, 1996.
20) Stoica P., and R.L. Moses, *Introduction to Spectral Analysis*, Prentice-Hall, Englewood Cliffs, NJ, pp. 52-54, 1997.
21) Welch P. D., *The Use of Fast Fourier Transform for the Estimation of Power Spectra: A Method Based on Time Averaging Over Short, Modified Periodograms*, IEEE Trans. Audio Electro Acoustics, Vol. AU-15, pp. 70-73, 1967.
22) Beskhyroun S., Mikami S., Oshima T. and Yamazaki T., Modified damage identification algorithm based on vibration measurements, *Journal of Applied Mechanics, JSCE*, Vol.7, pp. 97-107, 2004.
23) http://ext.lanl.gov/projects/damage_id/data2.htm.

(Received: April 15, 2005)